^{68}Ga-FAP-2286 PET of Solid Tumors: Biodistribution, Dosimetry, and Comparison with ^{18}F-FDG

Brad Kline[1], Surekha Yadav[1], Youngho Seo[1], Robin Cumming Ippisch[1], Jessa Castillo[1], Rahul R. Aggarwal[2], Robin Kate Kelley[2], Spencer C. Behr[1], Robert R. Flavell[1,2], Courtney Lawhn-Heath[1], Michelle Melisko[2], Hope S. Rugo[2], Victoria Wang[2], Sue S. Yom[3], Patrick Ha[4], Fei Jiang[5], and Thomas A. Hope[1]

[1]Department of Radiology and Biomedical Imaging, University of California San Francisco, San Francisco, California; [2]Helen Diller Comprehensive Cancer Center, University of California San Francisco, San Francisco, California; [3]Department of Radiation Oncology, University of California San Francisco, San Francisco, California; [4]Department of Otolaryngology–Head and Neck Surgery, University of California San Francisco, San Francisco, California; and [5]Department of Epidemiology and Biostatistics, University of California San Francisco, San Francisco, California

Fibroblast activation protein (FAP), expressed in the tumor microenvironment of a variety of cancers, has become a target of novel PET tracers. The purpose of this report is to evaluate the imaging characteristics of ^{68}Ga-FAP-2286, present the first—to our knowledge—dosimetry analysis to date, and compare the agent with ^{18}F-FDG and FAPI compounds. **Methods:** Patients were administered 219 ± 43 MBq of ^{68}Ga-FAP-2286 and scanned after 60 min. Uptake was measured in up to 5 lesions per patient and within the kidneys, spleen, liver, and mediastinum (blood pool). Absorbed doses were evaluated using MIM Encore and OLINDA/EXM version 1.1 using the International Commission on Radiological Protection publication 103 tissue weighting factor. **Results:** Forty-six patients were imaged with ^{68}Ga-FAP-2286 PET. The highest average uptake was seen in sarcoma, cholangiocarcinoma, and colon cancer. The lowest uptake was found in lung cancer and testicular cancer. The average SUV_{max} was significantly higher on ^{68}Ga-FAP-2286 PET than on ^{18}F-FDG PET in cholangiocarcinoma (18.2 ± 6.4 vs. 9.1 ± 5.0, $P = 0.007$), breast cancer (11.1 ± 6.8 vs. 4.1 ± 2.2, $P < 0.001$), colon cancer (13.8 ± 2.2 vs. 7.6 ± 1.7, $P = 0.001$), hepatocellular carcinoma (9.3 ± 3.5 vs. 4.7 ± 1.3, $P = 0.01$), head and neck cancer (11.3 ± 3.5 vs. 7.6 ± 5.5, $P = 0.04$), and pancreatic adenocarcinoma (7.4 ± 1.8 vs. 3.7 ± 1.0, $P = 0.01$). The total-body effective dose was estimated at 1.16E−02 mSv/MBq, with the greatest absorbed organ dose in the urinary bladder wall (9.98E−02 mGy/MBq). **Conclusion:** ^{68}Ga-FAP-2286 biodistribution, dosimetry, and tumor uptake were similar to those of previously reported FAPI compounds. Additionally, ^{68}Ga-FAP-2286 PET had consistently higher uptake than ^{18}F-FDG PET. These results are especially promising in the setting of small-volume disease and differentiating tumor from inflammatory uptake.

Key Words: dosimetry; FAP-2286; fibroblast activation protein; PET

J Nucl Med 2024; 65:938–943
DOI: 10.2967/jnumed.123.267281

Fibroblast activation protein (FAP)–targeting radioligands have emerged as promising agents in diagnostic cancer imaging and therapy. FAP is a transmembrane glycoprotein with a limited presence in healthy adult tissue but significant expression in cancer-associated fibroblasts, which are present in the stroma of most epithelial tumors and are known to be involved in disease growth and progression (*1*,*2*). The tumorigenic nature of cancer-associated fibroblasts, and the fact that they are absent from most healthy tissue, make FAP an attractive target in the development of pantumor radiopharmaceuticals.

Most of the literature on FAP-targeting PET focuses on the FAP inhibitors (FAPIs). FAPI-04, for example, has shown excellent uptake in breast cancer, esophageal cancer, lung cancer, sarcoma, and cholangiocarcinoma, as well as superior diagnostic efficacy in primary and metastatic lesions compared with ^{18}F-FDG across several tumor types (*3*,*4*). There is also considerable interest and promising results in abdominal malignancies and using FAPI tracers to identify peritoneal spread, which is poorly imaged with ^{18}F-FDG (*5*).

FAP-2286 differs from FAPI molecules using a cyclic peptide as a binding motif rather than a quinolone-based structure; however, previous evaluations have shown similar imaging characteristics to FAPI compounds (*6*). For example, Pang et al. recently presented results indicating the superiority of FAP-2286 over ^{18}F-FDG in hepatic, gastric, and pancreatic cancers (*7*). Preclinical and first-in-humans studies of ^{68}Ga-FAP-2286 and ^{177}Lu-FAP-2286 have also demonstrated prolonged tumor retention, making it a potential therapeutic target (*6*,*8*).

Here, we present our initial prospective experience with ^{68}Ga-FAP-2286, including comparison to ^{18}F-FDG PET when available, biodistribution in major organs, and radiation dosimetry analysis.

MATERIALS AND METHODS

Study Design and Patients

This single-arm, prospective study was performed at the University of California San Francisco with the approval of the local institutional review board (NCT04621435) and according to the ethical principles of the 1964 Declaration of Helsinki. Patients were eligible if they had histopathologically confirmed solid tumors. They were enrolled into cohort 1 (dosimetry cohort, which included patients with and without RECIST-measurable disease), cohort 2 (metastatic disease present on the basis of RECIST), or cohort 3 (no evidence of metastatic disease but at high risk for the presence of metastatic disease). All patients gave written informed consent. Data were collected in a central REDCap database. ^{18}F-FDG PET scans were included for comparison if

Received Dec. 22, 2023; revision accepted Mar. 25, 2024.
For correspondence or reprints, contact Thomas A. Hope (thomas.hope@ucsf.edu).
Published online May 2, 2024.

they were performed within 3 mo of the ^{68}Ga-FAP-2286 PET. Imaging results in patients with bladder cancer will be reported separately.

^{68}Ga-FAP-2286 Radiosynthesis

Radiosynthesis was conducted in an iQS ^{68}Ga fluidic labeling module and cassette (ITM Pharma Solutions GmbH). The precursor, FAP-2286 (Clovis Oncology, Inc.), was prepared into 41-μg/50-μL ultra-high-purity water aliquots and stored at −20°C until use. Before radiosynthesis, the precursor aliquot was mixed with 800 μL of 1 M ammonium acetate and 200 μL of 0.125 M sodium ascorbate. The reactor was preheated to 120°C, and the prepared precursor was added. ^{68}Ga was eluted from a ^{68}Ge/^{68}Ga generator (Eckert and Ziegler) with 5 mL of 0.1 M HCl into the reactor, yielding $^{68}GaCl_3$ with radioactivity in the range of 555–1,110 MBq (15–30 mCi). The radiolabeling proceeded for 10 min, and the reaction mixture was passed through a sterilizing filter into a sterile, pyrogen-free product vial to yield ^{68}Ga-FAP-2286. The radiolabeling yield was 95%, and radiochemical purity was 97% (n = 15).

^{68}Ga-FAP-2286 PET Imaging

Patients were injected with 219 ± 43 MBq (allowed range, 111–296 MBq) and imaged at a mean of 61 ± 7.4 min after injection with a target uptake time of 60 min (allowed range, 50–100 min). A subset of 10 patients was also imaged at 30 and 120 min for dosimetry. Patients were imaged on either a Vision PET/CT (n = 34, Siemens Healthineers) or a 3.0-T Signa PET/MRI (n = 12, GE Healthcare). For PET/CT, continuous bed motion was used with a bed speed of 0.7 cm/s, resulting in a scan duration of 11 min and 46 s for a coverage of 495.5 cm. Noncontrast low-dose CT was used for attenuation correction, and images were reconstructed using ultraHD•PET (Siemens) time of flight with 8 iterations and 5 subsets. For PET/MRI, a whole-body PET acquisition from the mid thighs to the vertex was obtained for 3 min at each of the 6 bed positions. The following MRI sequences were obtained at each bed position: axial MR attenuation correction and axial T1-weighted images (LAVA Flex; GE Healthcare).

Image Interpretation

A board-certified nuclear medicine physician evaluated the reconstructed PET, CT, or MR images. A positive lesion on PET was defined as a focus of activity with an SUV at least 1.5 times higher than the SUV_{mean} of the mediastinal blood pool and not attributable to physiologic distribution such as urinary excretion. A volume of interest was semiautomatically placed around each lesion, and the calculated SUV_{max} was recorded, including lesions that were detected on standard scans but were not positive on PET. SUV_{max} data were then averaged across all lesions within a given patient. To avoid clustering effects, analysis was limited to the 5 largest lesions in each individual patient. Additionally, volumes of interest were placed over the mediastinum, liver, spleen, and kidneys to measure physiologic distribution; SUV_{peak} was used for quantification in the kidneys. Quantitative uptake was performed at the 60-min time point for all patients.

Radiation Dosimetry

The 10 patients in the dosimetry cohort were imaged at 30-, 60-, and 120-min time points. The data from these patients were used to estimate the internal radiation dose. MIM Encore (MIM Software) was used to segment the source organs. All activity within each organ was included. OLINDA version 2.0 was used to derive values, with curve fitting performed on the EXM module of the OLINDA version 1.1 software package (*9*). The reference adult model with International Commission on Radiological Protection publication 103 tissue weighting factor was used (*10*).

Safety

The first 35 patients enrolled in the study underwent pre- and postimaging laboratory evaluation, electrocardiography, physical examination, and vital sign assessment. Subsequent patients underwent physical examination and vital sign assessment only. All patients were monitored for adverse events up to 2 h after injection and were contacted again 1–3 d later to evaluate for delayed adverse events.

Statistical Analysis

Descriptive statistics were used to describe uptake across tumor types. The Student t test was used for comparison of SUVs between ^{68}Ga-FAP-2286 and ^{18}F-FDG PET. P values of less than 0.05 were considered statistically significant.

RESULTS

Patient Characteristics and Safety

Forty-six patients were enrolled between January 2021 and April 2023. Patient characteristics are available in Table 1. No clinically significant changes were seen in laboratory assessments or electrocardiograms in the first 35 patients who received ^{68}Ga-FAP-2286. Across all patients, there were no clinically significant changes in physical examination findings or vital signs after administration. No serious adverse events were reported.

Biodistribution

SUV_{mean} was measured in the liver (2.0 ± 0.8), spleen (0.95 ± 0.31), and blood pool (1.4 ± 0.4), and SUV_{peak} was measured in the kidneys (4.2 ± 1.4), at the 60-min time point in all 46 patients (Supplemental Fig. 1; supplemental materials are available at http://jnm.snmjournals.org).

Tumor Uptake and Effect of Lesion Size

Forty-three patients had ^{68}Ga-FAP-2286–positive lesions, including all patients in cohort 1 and nearly all patients in cohort 2. Sarcoma (SUV_{max}, 16.8 ± 7.5) and cholangiocarcinoma (SUV_{max}, 16.6 ± 6.5) demonstrated the highest uptake across tumor types (Fig. 1). The total number of lesions evaluated was 147, with a distribution by lesion size as follows: 5 lesions measured 0–5 mm; 23 lesions, 5–10 mm; 33 lesions, 10–15 mm; 17 lesions, 15–20 mm; and 69 lesions, more than 20 mm. Median SUV_{max} generally increased with lesion size (Supplemental Fig. 2, P = 0.037 for the 0- to 5-mm and >20-mm groups).

Comparison to ^{18}F-FDG

Comparing ^{68}Ga-FAP-2286 PET with ^{18}F-FDG PET across all disease types, there was higher uptake on ^{68}Ga-FAP-2286 PET than on ^{18}F-FDG PET (11.5 ± 6.4 vs. 7.8 ± 5.9, P < 0.001; Fig. 2). The disease types with the highest relative uptake on ^{68}Ga-FAP-2286 PET compared with ^{18}F-FDG were cholangiocarcinoma (n = 4, 18.2 ± 6.4 vs. 9.1 ± 5.0, P = 0.007), breast cancer (n = 6, 11.1 ± 6.8 vs. 4.1 ± 2.2, P < 0.001), colon cancer (n = 1, 13.8 ± 2.2 vs. 7.6 ± 1.7, P = 0.001), HCC (n = 2, 9.3 ± 3.5 vs. 4.7 ± 1.3, P = 0.01), head and neck cancer (n = 6, 11.3 ± 3.5 vs. 7.6 ± 5.5, P = 0.04), and pancreatic adenocarcinoma (n = 1, 7.4 ± 1.8 vs. 3.7 ± 1.0, P = 0.01).

Dosimetry

The dosimetry is reported in Table 2 (full table available as Supplemental Table 1). The highest absorbed dose for ^{68}Ga-FAP-2286 was in the urinary bladder wall (9.98E−02 mGy/MBq), followed by the kidneys (4.31E−02 mGy/MBq), liver (2.23E−02 mGy/MBq), and spleen (7.9E−03 mGy/MBq). The effective dose was estimated at 1.16E−02 mSv/MBq.

TABLE 1
Patient Characteristics

Characteristic	Cohort 1	Cohort 2	Cohort 3	Overall
Number of patients	10	25	11	46
Sex (*n*)				
Female	5	12	6	23
Male	5	13	5	23
Age (y)				
Range	26–83	33–80	44–78	26–83
Median	67	60	63	64
Diagnosis (*n*)				
Breast cancer	1	5	3	9
Head/neck cancer	0	0	8	8
Sarcoma	2	6	0	8
Cholangiocarcinoma	4	1	0	5
Prostate cancer	1	4	0	5
HCC	1	2	0	3
Colon cancer	0	2	0	2
Pancreatic cancer	1	1	0	2
Lung cancer	0	2	0	2
Testicular cancer	0	1	0	1
Mesothelioma	0	1	0	1
Average administered activity (MBq)	228 ± 51	218 ± 41	212 ± 38	219 ± 43
Average uptake time (min)	59 ± 3.9	62.4 ± 8.8	61.6 ± 5.3	61 ± 7.4
Average time between ^{18}F-FDG and ^{68}Ga-FAP-2286 PET (d)	40 ± 24	42 ± 27	50 ± 35	44 ± 24

Clinical Applications of Note

A total of 8 patients with head and neck cancer were enrolled, 2 of whom had no evidence of disease. SUV_{max} in primary lesions was 13.1 ± 5.5 and uptake in metastases was 11.5 ± 3.7, and there was higher uptake in metastases with ^{68}Ga-FAP-2286 than with ^{18}F-FDG (11.5 vs. 5.6, $P < 0.001$). One benefit of ^{68}Ga-FAP-2286 compared with ^{18}F-FDG was relatively low background uptake in mucosal, salivary, and inflammatory regions of uptake. In one case, a patient at staging had false-positive nodes on ^{18}F-FDG PET due to a recent coronavirus disease 2019 vaccination; these nodes demonstrated no uptake on the ^{68}Ga-FAP-2286 PET (Fig. 3).

In total, 9 patients with breast cancer were enrolled. Lesion SUV_{max} was higher on ^{68}Ga-FAP-2286 PET than on ^{18}F-FDG PET in all patients (11.1 vs. 4.1, $P < 0.001$). The largest difference in SUV_{max} was in 2 patients with estrogen receptor–positive/progesterone receptor–positive/human epidermal growth factor receptor 2–negative invasive ductal carcinoma, for whom the highest lesion SUV_{max} was 23.2 and 17.9 on ^{68}Ga-FAP-2286 PET compared with 7.5 and 7.7 on ^{18}F-FDG PET. ^{68}Ga-FAP-2286 SUV_{max} was higher in patients with invasive ductal carcinoma ($n = 4$) than in patients with invasive lobular carcinoma (ILC) or mixed ductolobular carcinoma ($n = 5$) (SUV_{max} of 14.6 for invasive ductal carcinoma vs. 4.9 for ILC/mixed; $P = 0.046$).

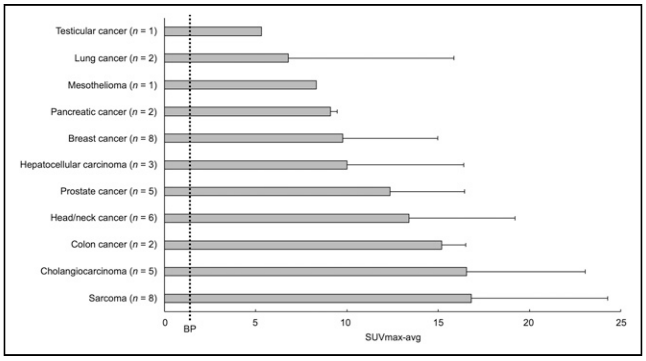

FIGURE 1. Tumor uptake by tumor type. SUV_{max}-avg represents average SUV_{max} of hottest lesion per patient. Error bars represent 95% CI. Average blood pool uptake (BP) was 1.4.

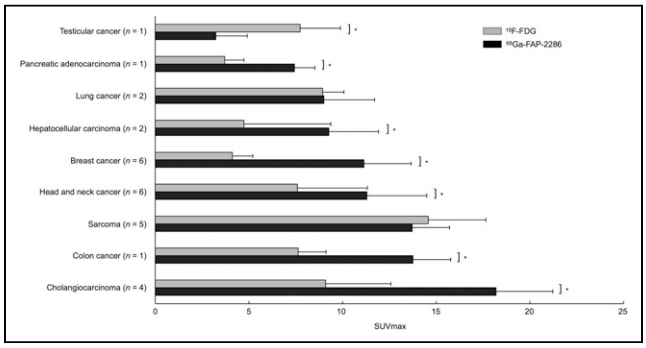

FIGURE 2. Comparison of paired SUV_{max} across various cancer types imaged with ^{68}Ga-FAP-2286 PET vs. ^{18}F-FDG PET. Error bars represent 95% CI. *$P < 0.05$.

TABLE 2
Selected Organ-Absorbed Dose and Effective Dose for ^{68}Ga-FAP-2286 and Other Tracers

Parameter	^{68}Ga-FAP-2286	^{68}Ga-FAPI-46 (*12*)	^{18}F-FDG (*20*)
Kidneys (mGy/MBq)	4.31E−02	1.60E−02	1.7E−02
Liver (mGy/MBq)	2.23E−02	1.01E−02	2.1E−02
Spleen (mGy/MBq)	7.93E−03	6.96E−03	1.1E−02
Urinary bladder wall (mGy/MBq)	9.98E−02	4.83E−02	1.3E−01
Effective dose (mSv/MBq)	1.16E−02	7.80E−03	1.9E−02
Typical injected activity			
MBq	229	236	370
mCi	6.18	6.38	10
Estimated effective dose per scan (mSv)	2.65	1.84	7.0

Anecdotally, the higher uptake on ^{68}Ga-FAP-2286 PET resulted in improved lesion visualization, particularly promising for ILC (Fig. 4).

In total, 5 patients with cholangiocarcinoma and 3 patients with hepatocellular carcinoma (HCC) were enrolled. The SUV_{max} in cholangiocarcinoma was higher than that in HCC (13.5 vs. 8.6, $P = 0.03$), although one HCC had an SUV_{max} of 15.8, overlapping with the cholangiocarcinoma patients. In patients for whom paired ^{18}F-FDG PET was available, both cholangiocarcinoma and HCC had higher uptake on ^{68}Ga-FAP-2286 PET than on ^{18}F-FDG PET (cholangiocarcinoma: 18.1 vs. 9.1, $P = 0.009$; HCC: 9.3 vs. 4.7, $P = 0.04$) (Fig. 5). There was no difference in uptake between intrahepatic cholangiocarcinoma lesions and extrahepatic disease (14.0 for intrahepatic vs. 12.7 for extrahepatic, $P = 0.7$).

DISCUSSION

Here, we report the results of patient imaging using ^{68}Ga-FAP-2286 PET. We evaluated biodistribution and dosimetry, which demonstrated that ^{68}Ga-FAP-2286 is excreted primarily via the kidneys and has a whole-body effective dose consistent with previously studied FAPI agents. Tumor uptake ranged from 5.3 to 16.8 and in general was higher on ^{68}Ga-FAP-2286 PET than on paired ^{18}F-FDG PET, although there was variation among tumor types.

The biodistribution of ^{68}Ga-FAP-2286 is similar to that of previously reported FAPI compounds, with low uptake in all organs except the kidney, consistent with predominate renal excretion. There was a slight increase in liver uptake and kidney uptake compared with the previously reported agents FAPI-04, FAPI-46, and FAPI-72 (*11*). This is similar to results reported by Pang et al., who also found that the biodistribution was similar between FAP-2286 and FAPI-46, with higher liver and kidney uptake (*7*). This was also consistent with our dosimetry analysis, which demonstrated a higher absorbed dose in the liver than was seen with ^{68}Ga-FAPI compounds (*12*,*13*), supporting greater hepatic accumulation. Overall, the average effective whole-body dose of ^{68}Ga-FAP-2286 PET was 1.16E−02 mSv/MBq, which is slightly lower than that of ^{18}F-FDG PET and similar to that of ^{68}Ga-FAPI-46 (*12*).

Uptake across tumor types was largely consistent with previous studies of FAPI compounds, including a study by Kratochwil et al. (*3*). In particular, colon and pancreatic cancer were significantly higher on ^{68}Ga-FAP-2286 PET than on ^{18}F-FDG PET, similar to what was found by Pang et al. (*7*), which may be attributable to the role of cancer-associated fibroblasts in the desmoplastic reactions surrounding pancreatic cancer cells, as well as the increased presence of fibroblasts in the tumor microenvironment of colon cancer (*14*,*15*). In our study, lesions were generally smaller than those reported previously because of cohort 3, which included patients without measurable disease and therefore biased our study toward smaller lesions. The smaller average lesion size could contribute to an underestimate of average SUV_{max}. This possibility is further supported by the similarity in median uptake between smaller lesions and larger ones. Lesions in the smallest grouping had a median SUV_{max}

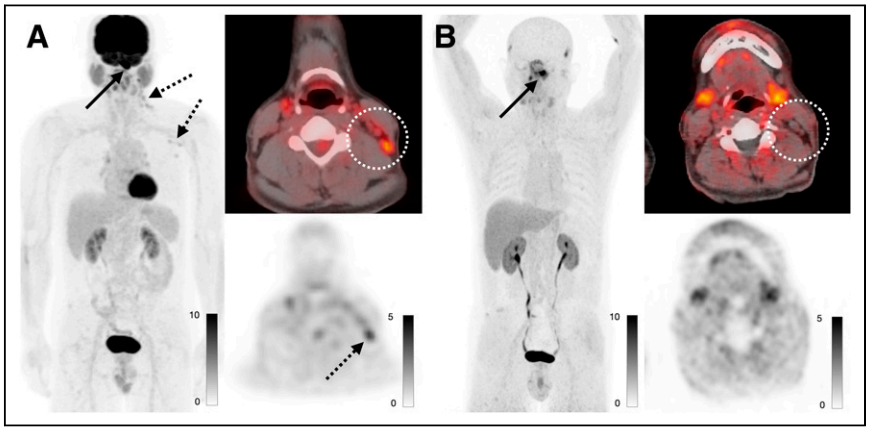

FIGURE 3. A 58-y-old man with newly diagnosed nasopharyngeal carcinoma. (A) Maximum-intensity projections, axial fused PET, and axial PET images from ^{18}F-FDG PET/CT demonstrate known nasopharyngeal mass with SUV_{max} of 23.7 (solid arrow), along with small but mildly hypermetabolic left cervical and axillary lymph nodes with SUV_{max} of up to 3.7 (dashed arrows, dotted circle). (B) Maximum-intensity projections, axial fused PET, and axial PET images from ^{68}Ga-FAP-2286 PET/CT demonstrate only nasopharyngeal mass with SUV_{max} of 12.7 (arrow), with no uptake in the cervical lymph nodes (dotted circle). Fine-needle aspiration of left cervical node revealed reactive changes, which was attributed to recent coronavirus disease 2019 vaccine.

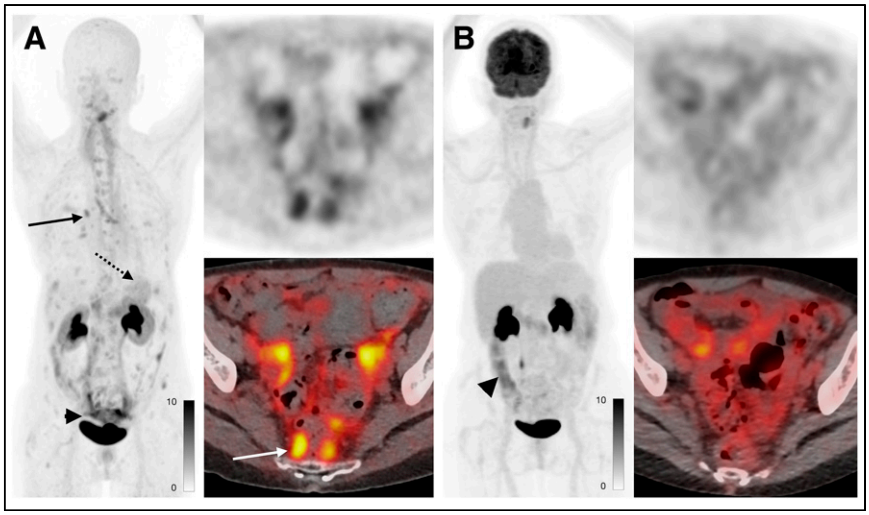

FIGURE 4. A 72-y-old woman with metastatic invasive lobular breast cancer. ^{68}Ga-FAP-2286 PET (A) revealed extensive metastatic disease not seen on ^{18}F-FDG PET (B), including small mediastinal and hilar lymph nodes (A, solid black arrow), diffuse gastric mucosal disease (A, dotted black arrow), and extensive peritoneal disease (SUV_{max}, 7.1; A, black arrowhead and white arrow). Uptake seen on ^{18}F-FDG PET in abdomen reflects physiologic uptake in bowel (B, black arrowhead) rather than tumor.

of 6.4, compared with 10.3 in the largest, potentially indicating good sensitivity for the detection of small sites of disease.

With head and neck cancer, uptake was greater than seen on ^{18}F-FDG PET, and maybe more importantly, there was anecdotal evidence that inflammatory nodes are not seen on ^{68}Ga-FAP-2286 PET, suggesting that ^{68}Ga-FAP-2286 may have value in nodal staging. Additionally, ^{68}Ga-FAP-2286 might better discriminate between the primary tumor and physiologic uptake in the oropharyngeal mucosa. Consistent with this possibility, previous work has shown that ^{68}Ga-FAPI-04 PET has higher sensitivity and specificity than ^{18}F-FDG PET for nodal metastases (*16*). In the setting of breast cancer, ^{68}Ga-FAP-2286 PET had higher uptake than ^{18}F-FDG PET, but this was particularly clinically relevant in ILC, for which disease frequently is not seen on ^{18}F-FDG PET (*17*). Previously, ILC that was ^{18}F-FDG–negative was shown to have uptake on ^{68}Ga-FAP-04 PET (*18*), and further work should be done in this setting. With liver tumors, there was hope that ^{68}Ga-FAP-2286 PET could help distinguish between HCC and cholangiocarcinoma. Although there was higher uptake in cholangiocarcinoma, there was overlap, which limited the ability of ^{68}Ga-FAP-2286 PET to help characterize intrahepatic lesions, as is consistent with results in prior work (*19*). One potential benefit of ^{68}Ga-FAP-2286 in cholangiocarcinoma could be the ability to distinguish between an adjacent tumor and inflammation associated with biliary ductal stents and obstruction, which is a common confounder with ^{18}F-FDG PET.

Limitations of our report include the small number of patients enrolled per cancer type, the absence of comparison to ^{18}F-FDG PET in some patients, and the possibility of disease progression within the 3-mo maximum time between ^{18}F-FDG PET and ^{68}Ga-FAP-2286 PET. Future studies with larger populations and smaller imaging windows would improve the robustness of our findings related to ^{68}Ga-FAP-2286 imaging. Additionally, ^{18}F-FDG PET was performed on different scanners, limiting the comparison between the ^{18}F-FDG and ^{68}Ga-FAP-2286 studies.

CONCLUSION

^{68}Ga-FAP-2286 biodistribution, dosimetry, and tumor uptake were similar to those of previously reported FAPI compounds. Additionally, ^{68}Ga-FAP-2286 PET had consistently higher uptake than ^{18}F-FDG PET. These results are especially promising in the setting of small-volume disease and differentiating tumor from inflammatory uptake.

DISCLOSURE

Thomas Hope has grant funding to the institution from Clovis Oncology, GE Healthcare, Lantheus, Janssen, Novartis, the Prostate Cancer Foundation, Telix Pharmaceuticals, and the National Cancer Institute (R01CA235741 and R01CA212148). He received personal fees from Bayer, Cardinal Health, BlueEarth Diagnostics, and Lantheus and received fees from and has an equity interest in RayzeBio and Curium. Robin Kelley has research funding to the institution from Agios, AstraZeneca, Bayer, BMS, Compass Therapeutics, Eli Lilly, EMD Serono, Exelixis, Genentech/Roche, Loxo Oncology, Merck, Novartis, Partner Therapeutics, QED, Relay Therapeutics, Servier, Surface Oncology, Taiho, and Tyra Biosciences. She received consulting/advisory fees from Compass, Exact Sciences, Kinnate, Regeneron, Tyra Therapeutics, and J-Pharma Inc. and to the institution from Agios, AstraZeneca, BMS, Exelixis, Ipsen, and Merck.

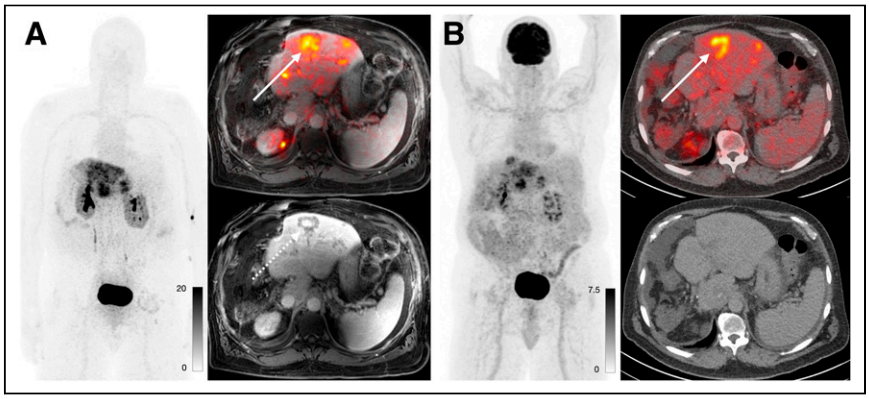

FIGURE 5. A 69-y-old man with cholangiocarcinoma imaged using PET/MRI. (A) ^{68}Ga-FAP-2286 images demonstrate uptake within hepatic metastases. Uptake is more central (solid arrow), which correlates with region of delayed enhancement on MRI (dashed arrow). (B) ^{18}F-FDG PET/CT demonstrates more peripheral uptake associated with more cellular component of tumor (arrow).

She received travel support from AstraZeneca and Merck. No other potential conflict of interest relevant to this article was reported.

KEY POINTS

QUESTION: What are the dosimetry and tumor uptake of ^{68}Ga-FAP-2286 PET?

PERTINENT FINDINGS: Our prospective study demonstrated a total-body effective dose of 1.16E−02 mSv/MBq and tumor uptake that mirrored that of other FAPI compounds. Additionally, ^{68}Ga-FAP-2286 PET had higher uptake than ^{18}F-FDG PET.

IMPLICATIONS FOR PATIENT CARE: In the setting of small-volume disease and differentiating tumor from inflammatory uptake, ^{68}Ga-FAP-2286 PET could improve staging.

REFERENCES

1. Loktev A, Lindner T, Mier W, et al. A tumor-imaging method targeting cancer-associated fibroblasts. *J Nucl Med.* 2018;59:1423–1429.
2. Garin-Chesa P, Old LJ, Rettig WJ. Cell surface glycoprotein of reactive stromal fibroblasts as a potential antibody target in human epithelial cancers. *Proc Natl Acad Sci USA.* 1990;87:7235–7239.
3. Kratochwil C, Flechsig P, Lindner T, et al. ^{68}Ga-FAPI PET/CT: tracer uptake in 28 different kinds of cancer. *J Nucl Med.* 2019;60:801–805.
4. Chen H, Pang Y, Wu J, et al. Comparison of [^{68}Ga]Ga-DOTA-FAPI-04 and [^{18}F] FDG PET/CT for the diagnosis of primary and metastatic lesions in patients with various types of cancer. *Eur J Nucl Med Mol Imaging.* 2020;47:1820–1832.
5. Zhao L, Pang Y, Luo Z, et al. Role of [^{68}Ga]Ga-DOTA-FAPI-04 PET/CT in the evaluation of peritoneal carcinomatosis and comparison with [^{18}F]-FDG PET/CT. *Eur J Nucl Med Mol Imaging.* 2021;48:1944–1955.
6. Zboralski D, Hoehne A, Bredenbeck A, et al. Preclinical evaluation of FAP-2286 for fibroblast activation protein targeted radionuclide imaging and therapy. *Eur J Nucl Med Mol Imaging.* 2022;49:3651–3667.
7. Pang Y, Zhao L, Meng T, et al. PET imaging of fibroblast activation protein in various types of cancer using ^{68}Ga-FAP-2286: comparison with ^{18}F-FDG and ^{68}Ga-FAPI-46 in a single-center, prospective study. *J Nucl Med.* 2023;64:386–394.
8. Baum RP, Schuchardt C, Singh A, et al. Feasibility, biodistribution, and preliminary dosimetry in peptide-targeted radionuclide therapy of diverse adenocarcinomas using ^{177}Lu-FAP-2286: first-in-humans results. *J Nucl Med.* 2022;63:415–423.
9. Stabin MG, Sparks RB, Crowe E. OLINDA/EXM: the second-generation personal computer software for internal dose assessment in nuclear medicine. *J Nucl Med.* 2005;46:1023–1027.
10. *ICRP Publication 103: The 2007 Recommendations of the International Commission on Radiological Protection.* International Commission on Radiological Protection; 2007.
11. Giesel FL, Kratochwil C, Schlittenhardt J, et al. Head-to-head intra-individual comparison of biodistribution and tumor uptake of ^{68}Ga-FAPI and ^{18}F-FDG PET/CT in cancer patients. *Eur J Nucl Med Mol Imaging.* 2021;48:4377–4385.
12. Meyer C, Dahlbom M, Lindner T, et al. Radiation dosimetry and biodistribution of ^{68}Ga-FAPI-46 PET imaging in cancer patients. *J Nucl Med.* 2020;61:1171–1177.
13. Giesel FL, Kratochwil C, Lindner T, et al. ^{68}Ga-FAPI PET/CT: biodistribution and preliminary dosimetry estimate of 2 DOTA-containing FAP-targeting agents in patients with various cancers. *J Nucl Med.* 2019;60:386–392.
14. Kamali Zonouzi S, Pezeshki PS, Razi S, Rezaei N. Cancer-associated fibroblasts in colorectal cancer. *Clin Transl Oncol.* 2022;24:757–769.
15. Nielsen MFB, Mortensen MB, Detlefsen S. Key players in pancreatic cancer-stroma interaction: cancer-associated fibroblasts, endothelial and inflammatory cells. *World J Gastroenterol.* 2016;22:2678–2700.
16. Jiang Y, Wen B, Li C, et al. The performance of ^{68}Ga-FAPI-04 PET/CT in head and neck squamous cell carcinoma: a prospective comparison with ^{18}F-FDG PET/CT. *Eur J Nucl Med Mol Imaging.* 2023;50:2114–2126.
17. Hogan MP, Goldman DA, Dashevsky B, et al. Comparison of ^{18}F-FDG PET/CT for systemic staging of newly diagnosed invasive lobular carcinoma versus invasive ductal carcinoma. *J Nucl Med.* 2015;56:1674–1680.
18. Eshet Y, Tau N, Apter S, et al. The role of ^{68}Ga-FAPI PET/CT in detection of metastatic lobular breast cancer. *Clin Nucl Med.* 2023;48:228–232.
19. Guo W, Pang Y, Yao L, et al. Imaging fibroblast activation protein in liver cancer: a single-center post hoc retrospective analysis to compare [^{68}Ga]Ga-FAPI-04 PET/CT versus MRI and [^{18}F]-FDG PET/CT. *Eur J Nucl Med Mol Imaging.* 2021;48:1604–1617.
20. Brix G, Lechel U, Glatting G, et al. Radiation exposure of patients undergoing whole-body dual-modality ^{18}F-FDG PET/CT examinations. *J Nucl Med.* 2005;46:608–613.